Surface Plasmon Resonance of Silver Nanoparticles on Vanadium Dioxide

Gang Xu,*,† Yong Chen,† Masato Tazawa,‡ and Ping Jin*,‡

Guangzhou Institute of Energy Conversion, Chinese Academy of Sciences, Guangzhou 510640, China, and National Institute of Advanced Industrial Science and Technology, Nagoya 463-8560, Japan

Received: October 9, 2005; In Final Form: December 12, 2005

The localized surface plasmon resonance (SPR) spectrum of silver nanoparticles fabricated on a thermochromatic film, vanadium dioxide (VO_2), is studied in this paper. Owing to the temperature-dependent dielectric function of VO_2, the SPR band dramatically exhibits temperature dependence in the range of 30−80 °C. The peak extinction wavelength, λ_{SPR}, blueshifts as temperature increases and reversibly redshifts as temperature decreases. The shift magnitude ($\Delta\lambda_{SPR}$) is strongly dependent on the silver mass thickness, d_m; a value of 50 nm of $\Delta\lambda_{SPR}$ is achieved for particles (mean diameter 51 nm) with $d_m = 2$ nm while a value of 250 nm is achieved for particles (mean diameter 133 nm) with $d_m = 10$ nm. Beyond the SPR band, it is interesting to find that the spectral line shape of silver particles is dominated by the imaginary part of the dielectric function of VO_2. These results can be interpreted based on dynamical Maxwell−Garnett theory.

Introduction

The absorption spectrum of noble metal nanoparticles is characterized by an anomalous adsorption band in the visible region that is absent in the bulk metal.[1] This band is ascribed to surface plasmon oscillation modes of conduction electrons in response to optical excitation, often called localized surface plasmon resonance (SPR). SPR excitation not only results in wavelength-selective photon absorption and scattering but also leads to dramatic enhancement of the local electromagnetic field near the surface of the nanoparticles. Such unique optical features make metal nanoparticles extremely valuable in a wide range of technological applications, such as optical devices,[2,3] plasmonics,[4,5] chemical and biological sensors,[6−9] various surface enhanced spectroscopies,[10,11] and so on.

It is well established that the SPR band is highly sensitive to the particle size, shape, spacing, filling factor (i.e., volume fraction), and composition as well as the surrounding dielectric medium.[1,12] Any change in these parameters would cause some interesting optical phenomena to be observed, particularly a corresponding shift in the peak extinction wavelength, λ_{SPR}. It is of great technological and intellectual value to understand these phenomena and to control the λ_{SPR}. Effects of the surrounding medium have been extensively studied. Nanoparticles supported by different substrates or embedded in different matrixes,[1,8,13−15] either homogeneous or heterogeneous, are different in λ_{SPR}. Particularly, λ_{SPR} sensitivity to the nanoenvironment (e.g., molecules adsorbed on the particle surface) provides the possibility to develop a new class of nanosensors.[6−9] Also, it has been found that a chemical contribution from the surrounding medium may strongly affect the SPR band if the particle diameter falls in the intrinsic size region (15 nm for Ag and 25 nm for Au).[8,9,16,17] Formation of a core−shell structure of the nanoparticles has been demonstrated to be an effective method for λ_{SPR} tuning.[18−20] Either the core or the shell can be the metal and the other is an insulator or a different metal. Wavelength tunability is achieved by varying the relative dimensions of the core and shell. Alloying the metal particles, e.g., Ag−Au,[21−23] Ag−Al,[24] etc., allows a certain control over the value of λ_{SPR}; λ_{SPR} in this case is a function of their mole fraction. A much more drastic effect on λ_{SPR} is found if the particle shape is changed. Rod-shaped nanoparticles with variable aspect ratios have been produced with a variety of procedures.[25−27] With the advent of some new synthetic methods including nanosphere lithography[14,28] and the wet-chemistry method,[26,29,30] which produce well-defined sizes and nonspherical shapes, control of the particle geometry recently became increasingly active. Interpreting the spectra also provides important challenges to electrodynamic theory.[31]

In this paper, we study the SPR spectra of silver nanoparticles fabricated on a thermochromatic metal oxide, VO_2, which exhibits a reversible metal−semiconductor phase transition at about 68 °C.[32] It is interesting to find that the SPR wavelength, λ_{SPR}, exhibits remarkable temperature dependence. A blue shift of 250 nm in λ_{SPR} has been observed for silver particles with a mass thickness of 10 nm when temperature increases from 30 to 80°C. Furthermore, this shift is thermally reversible and can be fine-tuned by temperature. In addition, we found that a nonvanishing imaginary part of the dielectric constant of the substrate strongly influences the line shape of the SPR spectrum. We use the dynamic Maxwell−Garnett theory to explain the observations.

Experimental Section

Both silver nanoparticles and VO_2 film were prepared by the radio frequency (rf) magnetron sputter method. The sputter system consists of a cylindrical chamber connecting to a turbo molecular pump with two 2-in. magnetron sources positioned upward at a 30° inclination to a rotatable substrate holder. The chamber was evacuated to 2×10^{-6} Pa, and pure Ar (99.9995%) was introduced at 30 sccm (standard cubic centimeters) to a pressure of 0.6 Pa. The VO_2 film was formed by reactive sputtering of a vanadium disk ($\phi = 50$ mm, 99.99% purity) with oxygen injection of 2.1 sccm at a substrate temperature of 500 °C. A sapphire (0001) slide ($20 \times 10 \times 0.3$ mm^3) was

* Corresponding authors. E-mail: xugang@ms.giec.ac.cn and p-jin@aist.go.jp.
† Guangzhou Institute of Energy Conversion.
‡ National Institute of Advanced Industrial Science and Technology.

10.1021/jp055744j CCC: $33.50
Published on Web 01/14/2006

used as the substrate. After deposition, this slide was cut into several pieces to ensure identical optical quality when they were subsequently used as the substrates for silver particles. Characterization of these films was reported previously.[33] The thickness of these VO_2 films was about 50 nm.

Silver nanoparticles were fabricated also in this system by sputtering a high purity silver disk ($\phi = 50$ mm, 99.99% purity) at room temperature in Ar atmosphere (0.6 Pa). The substrates, VO_2 coated sapphire, were ultrasonically cleaned in acetone and subsequently in ethanol for 15 min, respectively, and then dried with pure nitrogen flow. The amount of Ag impinging on the substrate was recorded with a quartz crystal oscillator, which was converted to an equivalent mass thickness for an ideal continuous film with bulk density. The silver island films were then annealed at 500 °C for 10 min in a vacuum.

Atomic force microscope (AFM) images are collected on a Nanoscope III scanning probe microscope (Digital Instruments) operated in tapping mode under ambient conditions. Etched Si nanoprobe tips (TAP 300, Nanodevices) with a spring constant of 40 N/m and resonance frequency of 300 kHz ± 100 kHz were used. The dielectric functions of the VO_2 thin film are precisely determined with a spectroscopic ellipsometer (M2000VI, J. A. Woollam). The extinction spectra are recorded on a UV−Vis−NIR spectrophotometer (V-570, Jasco) with an attachment (ETC-505) to control temperature. One of the cut pieces of VO_2-coated sapphire without silver was used as a reference.

Dynamical Maxwell−Garnett Theory

The Maxwell−Garnett (MG) theory has been successfully applied to interpret the optical properties of composite materials including metallic island films.[34,35] As a first-order approximation, this theory is equivalent to dipole−dipole coupling, and convenient to describe the effects of the particle filling factor on λ_{SPR}. Conventional MG theory is only valid in the "quasistatic" regime characterized by $r/\lambda \leq 0.01$, where r is the radius of the metal particle and λ is the wavelength of light. In this theory, the composite is characterized by an effective complex dielectric function, $\tilde{\epsilon}$, at any λ. $\tilde{\epsilon}$ is given by

$$\frac{\tilde{\epsilon} - \tilde{\epsilon}_{ext}}{L\tilde{\epsilon} + (1+L)\tilde{\epsilon}_{ext}} = q\frac{\tilde{\epsilon}_m - \tilde{\epsilon}_{ext}}{L\tilde{\epsilon}_m + (1-L)\tilde{\epsilon}_{ext}} \quad (1)$$

where q is the particle filling factor and L is the depolarization factor characterizing the shape of the metal particles. $\tilde{\epsilon}_m$ and $\tilde{\epsilon}_{ext}$ are the complex dielectric functions of the metallic particles and external surrounding medium, respectively. For metallic particles on a substrate ($\tilde{\epsilon}_{sub}$), $\tilde{\epsilon}_{ext}$ may be simply given as

$$\tilde{\epsilon}_{ext} = \sigma\tilde{\epsilon}_{sub} + (1+\sigma)\tilde{\epsilon}_{air} \quad (2)$$

contributions from both the substrate and air ($\tilde{\epsilon}_{air} = 1$) weighted by a factor σ ($0 \leq \sigma \leq 1$), defined as the ratio of the particle contact area with the substrate to the particle surface area. Empirically, it was assumed that $\tilde{\epsilon}_{ext} = (\tilde{\epsilon}_{sub} + 1)/2$, i.e., $\sigma = 0.5$, an average of the contributions from the substrate and the air. Actually, the real value of σ is associated with how the particles sit on the substrate.

Recently, Martin et al.[25] propose a dynamical MG model applicable for large particles. In this model, the depolarization factor L in eq 1 is replaced by a complex and wavelength-dependent L_{eff}, which is related to the particle's radius a via

$$L_{eff} = L - \frac{1}{3}k^2a^2 - \frac{2}{9}i\tilde{k}^3a^3 \quad (3)$$

TABLE 1: Summary of the Parameters of Silver Nanoparticles with Mass Thickness $d_m = 2$, 6, and 10 nm

	$d_m = 2$ nm	$d_m = 6$ nm	$d_m = 10$ nm[a]
mean diameter, $2a$ (nm)	51 ± 15	96 ± 23	133 ± 53
mean height, $2c$ (nm)	45 ± 11	88 ± 9	42 ± 14
filling factor, q[b]	0.08	0.15	0.28
λ_{SPR}(S phase) (nm)	650	686	956
λ_{SPR}(M phase) (nm)	600	620	704
$\Delta\lambda_{SPR}$ (nm)	50	66	252
area ratio, σ	0.32	0.21	0.08

[a] Particle diameter was calculated by converting the area of the particle top surface to that of a circle. [b] Calculated according to ref 35c for the cases $d_m = 2$ and 6 nm. For the case $d_m = 10$ nm, q is simply equated to the area ratio of the particles to the substrate.

where $\tilde{k} = 2\pi a\tilde{n}_{ext}/\lambda$ with $\tilde{n}_{ext}^2 = \tilde{\epsilon}_{ext}$. Thus, the shape and retardation effects of large particles as well as the damping of the induced dipole due to radiation emission are all included in L_{eff}. Such treatment substantially is equal to the modified long wavelength approximation (MLWA),[31] which considers the finite wavelength effects in the quasistatic regime. For oblate spheroids,[34] L is given by

$$L = \frac{1}{2}\left[1 - \frac{1+e^2}{e^3}(e - \tan^{-1}e)\right] \quad (4)$$

where e is the eccentricity defined as $e = [(a/c)^2 - 1]^{1/2}$ with c the semiminor axis of the particles (perpendicular to the film surface).

Once the effective complex dielectric function $\tilde{\epsilon}$ at any λ has been obtained, the extinction spectrum, E, of the SPR can be calculated by $E = \log(T_{Ag}/T_0)$, in which T_{Ag} and T_0 are the transmittance of multilayer, the former containing the effective medium layer (silver nanoparticles) and the latter silver free. The optical calculation for multilayer was performed with a transfer matrix method.

Results and Discussion

Silver nanoparticles with mass thickness $d_m = 2$, 6, and 10 nm are prepared. Their AFM images ($5 \times 5\ \mu m^2$) are shown in Figure 1, parts a, b, and c, respectively. The corresponding size histograms are depicted in the left column of Figure 1, parts d, e, and f. Table 1 summarizes the data concerning the particles of the three samples. It shows that the particle filling factor, mean diameter, and height all increase with increasing mass thickness. For the cases $d_m = 2$ and 6 nm, the particles are nearly spherical whereas for $d_m = 10$ nm it is interesting to find that the particles show a variety of shapes but mainly in quadrilaterals and hexagons.

Figure 2 shows the dielectric constants of fabricated VO_2 film for its two phases, the semiconductor (S) phase at 30 °C and the metal (M) phase at 80 °C. The S−M transition centers at about 60 °C, but experiences quite a wide temperature interval, from 40 to 80 °C. This phase transition leads to a remarkable change in the film dielectric functions ($\epsilon_1 + i\epsilon_2$), as shown in Figure 2 (upper part for ϵ_1 and lower part for ϵ_2). In the S phase, the film exhibits a large and positive ϵ_1 and a moderately large ϵ_2, characteristic of a semiconductor; in the M phase, ϵ_1 decreases with wavelength and becomes negative in the IR region while ϵ_2 increases rapidly with wavelength, characterized by a metal. Notice an absorption peak on the curve of ϵ_2 for both phases. This peak locates at ~400 nm in wavelength.

The measured extinction spectra of the three samples with silver mass thickness $d_m = 2$, 6, and 10 nm are present in Figure 3, parts a, b, and c, respectively. The solid curves are the results

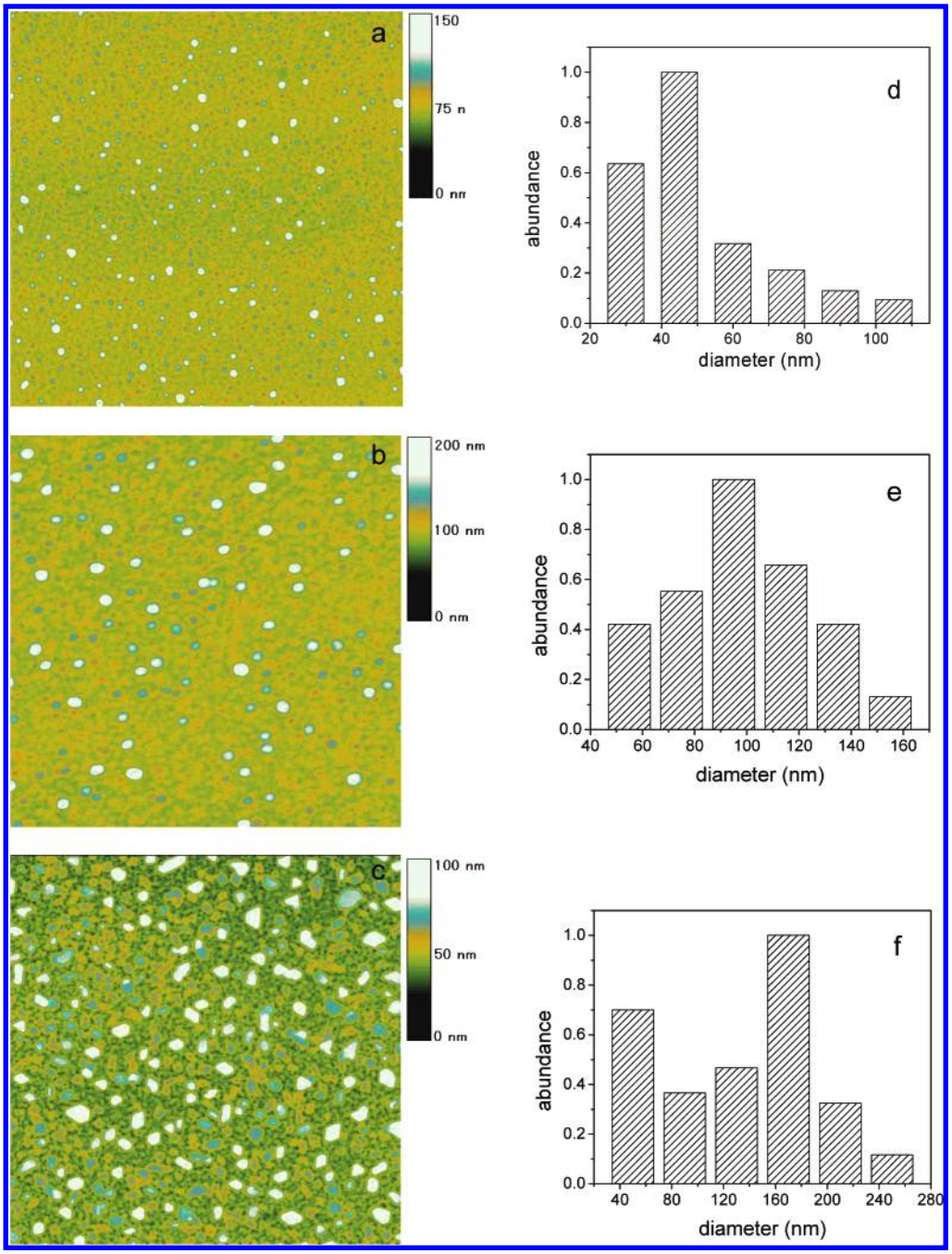

Figure 1. AFM images ($5 \times 5\ \mu m^2$) of silver nanoparticles with mass thickness $d_m = 2$ (a), 6 (b), and 10 nm (c). The corresponding size histograms are given in parts d−f, respectively. All the parameters of particles are tabulated in Table 1.

measured at 30 °C while the dashed curves are measured at 80 °C, which corresponds to the S and M phases of VO_2, respectively. As seen, the temperature effect on the peak extinction wavelength, λ_{SPR}, is pronounced. λ_{SPR} shifts to shorter wavelength when temperature increases from 30 to 80 °C for all three samples. It is well established that the SPR of noble metallic particles only shows a very small temperature effect due to the fact that the dominant electronic dephasing mechanism involves electron−electron interactions rather than electron−phonon coupling.[36] Therefore, we undoubtedly believe that what we observed originated from the change in dielectric constant of the supporting material, VO_2.

The effect of the mass thickness, d_m, is clear. Increase in d_m not only leads to a red shift of λ_{SPR} for both the S and M phases, but also enhances the difference in λ_{SPR} between the two phases. For the case $d_m = 2$ nm, for instance, the SPR wavelengths, λ_{SPR}, are respectively 650 nm for the S phase and 600 nm for the M phase, with the difference, $\Delta\lambda_{SPR}$, being 50 nm. In the case of $d_m = 10$ nm, the corresponding wavelengths are respectively 956 and 704 nm, with $\Delta\lambda_{SPR} = 252$ nm. The red shift is always observed for metallic island films formed through a natural growth process, e.g., thermal evaporation. This shift is attributed to the dipole−dipole interaction, which becomes more significant for larger particles and shorter interparticle spacing, a consequence of increasing d_m, as exhibited in Figure 1. The enhancement in $\Delta\lambda_{SPR}$ is due to the increasing difference in ϵ_1 between the two phases of VO_2 when wavelength increases, as shown in Figure 2 (upper part).

Additionally, we find that the spectral line shape of SPR is strongly affected by ϵ_2 of VO_2, which is supported by two facts. First, we note that the spectral line in the right side of SPR goes upward for the M phase, in accord with the situation of ϵ_2

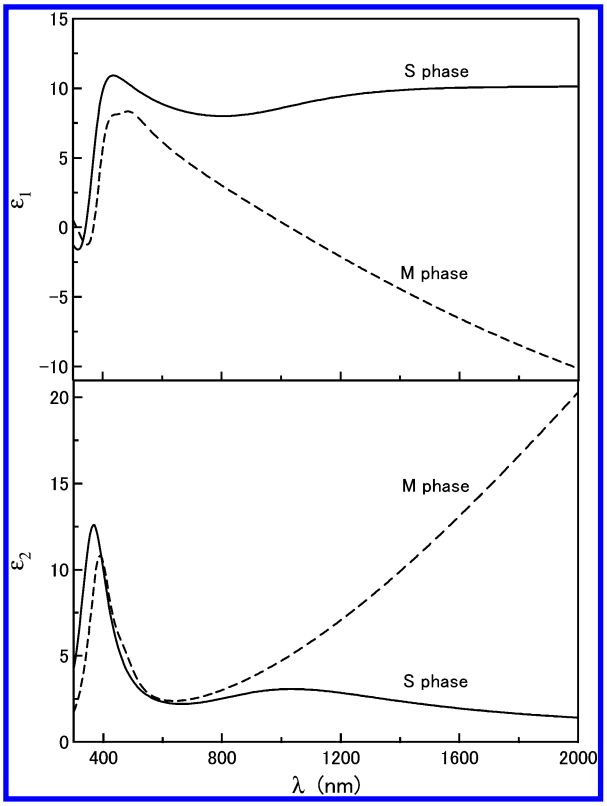

Figure 2. Dielectric functions of VO_2 thin film for its semiconductor (S) and metallic (M) phases: real parts (upper) and imaginary parts (lower). The S and M phases are measured at 30 and 80 °C, respectively.

of VO_2, as shown in Figure 2 (lower part). Second, an absorption peak located at $\lambda = 400$ nm is always present in the extinction spectrum. Its position and shape are affected neither by temperature nor by silver mass thickness, which behaves differently from the SPR band. We believe, as will be discussed, that this peak results from the substrate, rather than the silver particles. Actually, we notice two peaks in the dispersion curves of ϵ_2 of VO_2 for its two phases though the two peaks fail in coinciding due to a measurement error. Such error will be carried into our calculated spectra if these dielectric constants are used.

The simulated spectra for $d_m = 2$, 6, an 10 nm are presented in the right column of Figure 3, parts d, e, and f, respectively. The solid curves correspond to the S phase and the dashed curves to the M phase. The calculation was done according to eqs 1−4 together with the knowledge of the parameters of the silver particles (Table 1) and the dielectric constants of VO_2 (Figure 2). The optical constant of bulk silver was taken form ref 37 without considering the size effects. Particle size distribution is not considered, which mainly affects the bandwidth of SPR. Only the factor σ that represents the contact area is adjusted in the simulation to make the calculated $\Delta\lambda_{SPR}$ between the two phases match the value obtained experimentally. The values of σ for each case are tabulated in Table 1. One can see that the calculated spectra are in good agreement with the experimental spectra. The important features of the obtained data can be well predicted by dynamic MG theory, including the shift of λ_{SPR}, the spectral line shape, and the extra peak at ∼400 nm.

Notice σ is the only parameter through which effects of VO_2 are introduced (see eq 2). Its value determines not only $\Delta\lambda_{SPR}$ but also the specific position of λ_{SPR} for the two phases. Increase in σ favors the red shift of λ_{SPR} of the two phases and enhances their difference. Results reveal that σ decreases with increasing d_m, as exhibited in Table 1, which means that contributions from VO_2 diminish when silver particles get larger. It seems that the contact area of particle to substrate does not increase as rapidly as the particle size, probably due to the dewetting mechanism of the Ag film subjected to thermal annealing.[38] However, more details concerning metallic particles sitting on a rough substrate surface are needed experimentally.

$\Delta\lambda_{SPR}$ between the two phases does not decrease with the decrease in σ because $\Delta\lambda_{SPR}$ is also determined by $\Delta\epsilon_1$, the difference in ϵ_1 between the two phases of VO_2, in addition to σ. From Figure 2, $\Delta\epsilon_1$ increases with wavelength. That is to say, when the SPR band shifts to the infrared, contributions from $\Delta\epsilon_1$ play the dominant role relative to σ and make the case we obtained.

On the other hand, we find that the peak at ∼400 nm is determined by σ alone. It becomes very strong when $\sigma = 1$ and disappears when $\sigma = 0$. This confirms our assumption concerning the origin of this peak. So, the magnitude of σ, i.e., the contribution of VO_2 in the surrounding medium, is reflected by this peak. As we stated above, contribution from VO_2 diminishes when silver particles get larger. Indeed, we observed the reduction of this peak in the simulated spectra as d_m increases, which is basically consistent with the value measured, as shown in Figure 3.

It is interesting to note the transfer of the absorption properties of VO_2 into the SPR spectrum. It is seemingly unreasonable since all the spectra have been referenced to that of the substrate (VO_2/sapphire) during the measurements, as is commonly done for silver on glass. However, MG theory does demonstrate this truth and an explanation can be given accordingly; the supported silver particles form an effective medium with their surroundings and can*not* be looked as isolated. This means that cautions should be taken when one interprets the optical properties of metallic nanoparticles surrounded by or contacting an absorbing medium.

A fine-tuning of the temperature-dependent shift in λ_{SPR} is achievable in view of the fact that the phase transition of thin VO_2 films is smeared out over a broad temperature interval. Figure 4 shows such a measurement for the silver particles with $d_m = 10$ nm in which temperature is increased in a stepwise manner from 30 to 80 °C. In this case λ_{SPR} blue shifts as a function of temperature. A similar result can be obtained if temperature decreases in such a manner. Note again that the peak at ∼400 nm does not shift at any temperature.

Conclusions

In conclusion, we studied the localized surface plasmon resonance (SPR) spectrum of silver nanoparticles on a thermochromic material, vanadium dioxide (VO_2). The SPR band thereby exhibits drastic temperature effects due to the temperature-dependent dielectric constants of VO_2. The peak extinction wavelength shifts with temperature. This shift becomes more pronounced for silver particles with a larger mass thickness, d_m. A blue shift of 250 nm was observed for $d_m = 10$ nm when temperature increases from 30 to 80 °C and this shift is reversible when temperature decreases. Moreover, a fine-tuning of the shift is obtainable if temperature is controlled to increase or decrease in a stepwise manner. In addition, we find that an absorbing substrate has appreciable effects on the spectral line shape of the SPR spectrum.

Our study presented here actually opens a new way to manipulate the SPR, characterized by a large tunable wavelength range, thermal reversibility, and capability of fine-tuning. Note that such tuning can be carried out with only one sample by just changing its temperature and leaving the surface morphol-

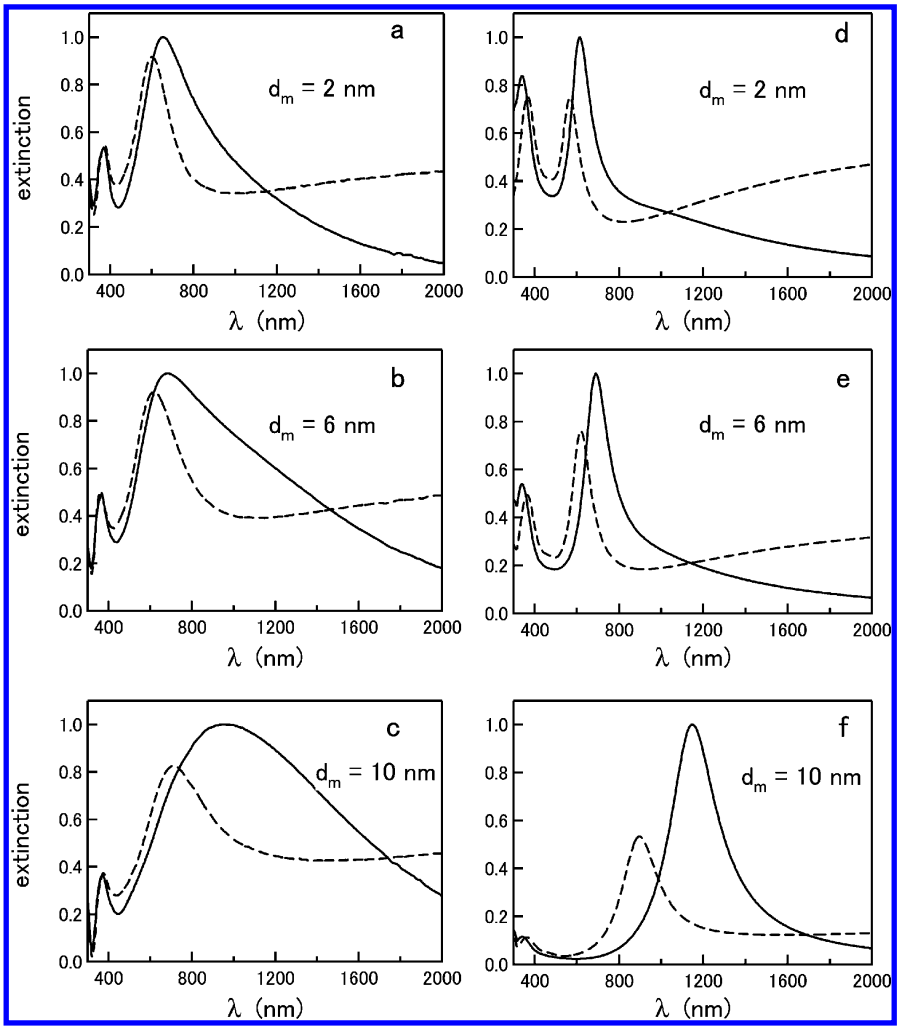

Figure 3. Experimental extinction spectra of the three samples with mass thickness $d_m = 2$ (a), 6 (b), and 10 nm (c) for both the S (solid curves) and M (dashed curves) phases. The corresponding simulated spectra with dynamic MG theory are given in parts d−f, respectively. In each case, the spectra are normalized to the S phase for comparison.

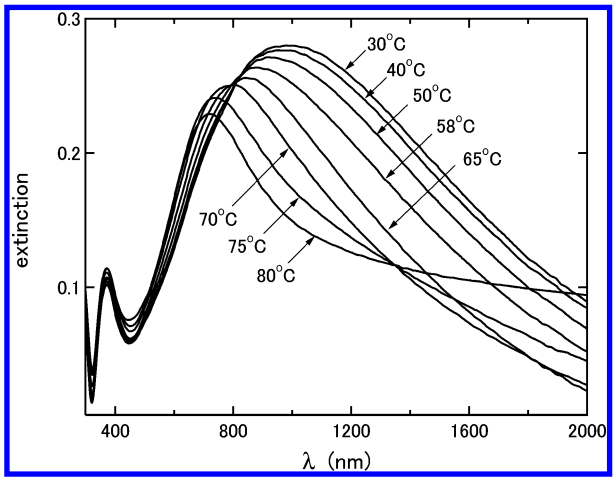

Figure 4. An example of fine-tuning of the SPR band for the sample with $d_m = 10$ nm. Note that the peak extinction wavelength is a function of temperature.

ogy of the particles unchanged. This undoubtedly benefits any optical application of metallic nanoparticles. For example, it allows an optical filer to work at diverse wavelengths. For chemical or biological sensors, we can readily tune the SPR to make the detection system work at the wavelength of highest sensitivity. In SES, we can tune the SPR frequency to match a given laser excitation frequency to obtain the highest enhancement factors. In particular, our method of wavelength tuning may provide a solution to the problem of reproducing surface morphology in understanding the mechanism of SERS.

Acknowledgment. This work is part of the research program of the One-Hundred Talent Project financially supported by the Chinese Academy of Science.

References and Notes

(1) Kreibig, U.; Vollmer, M. *Optical Properties of Metal Clusters*; Springer-Verlag: Heidelberg, Germany, 1995; Vol. 25.

(2) Dirix, Y.; Bastiaansen, C.; Caseri, W.; Smith, P. *Adv. Mater.* **1999**, *11*, 223.

(3) Gotschy, W.; Vonmetz, K.; Leitner, A.; Aussenegg, F. R. *Opt. Lett.* **1996**, *21*, 1099.

(4) (a) Nikolajsen, T.; Lessson, K.; Salakhutdinov, I.; Bozhevolnyi, S. I. *Appl. Phys. Lett.* **2003**, *82*, 668. (b) Bozhevolnyi, S. I.; Erland, J.; Leosson, K.; Skovgaard, P. M. W. *Phys. Rev. Lett.* **2001**, *86*, 3008.

(5) Barnes, W. L.; Dereux, A.; Ebbesen, T. W. *Nature* **2003**, *424*, 824.

(6) (a) Malinsky, M. D.; Kelly, K. L.; Schatz, G. C.; Van Duyne, R. P. *J. Am. Chem. Soc.* **2001**, *123*, 1471. (b) Haes, A. J.; Van Duyne, R. P. *J. Am. Chem. Soc.* **2002**, *124*, 10596. (c) Haynes, C. L.; Van Duyne, R. P. *J. Phys. Chem. B* **2001**, *105*, 5599.

(7) (a) Mirkin, C. A.; Letsinger, R. L.; Mucic, R. C.; Storhoff, J. J. *Nature* **1996**, *382*, 607. (b) Elghanian, R.; Storhoff, J. J.; Mucic, R. C.; Letsinger, R. L.; Mirkin, C. A. *Science* **1997**, *277*, 1078. (c) Cao, Y. W.; Jin, R.; Mirkin, C. A. *J. Am. Chem. Soc.* **2001**, *123*, 7961.

(8) (a) Hövel, H.; Fritz, S.; Hilger, A.; Kreibig, U.; Vollmer, M. *Phys. Rev. B* **1993**, *48*, 18178. (b) Kreibig, U.; Gartz, M.; Hilger, A. *Ber. Bunsen-Ges. Phys. Chem.* **1997**, *101*, 1593. (c) Hilger, A.; Cuppers, N.; Tenfelde, M.; Kreibig, U. *Eur. Phys. J. D* **2000**, *10*, 115.

(9) Henglein, A.; Meisel, D. *J. Phys. Chem. B* **1998**, *102*, 8364.
(10) Moskovits, M. *Rev. Mod. Phys.* **1985**, *57*, 783.
(11) (a) Van Duyne, R. P.; Hulteen, J. C.; Treichel, D. A. *J. Chem. Phys.* **1993**, *99*, 2101. (b) Jensen, T. R.; Van Duyne, R. P.; Johnson, S. A.; Maroni, V. A. *Appl. Spectrosc.* **2000**, *54*, 371. (c) Emory, S. R.; Nie, S. *J. Phys. Chem. B* **1998**, *102*, 493.
(12) Kelly, K. L.; Coronado, E.; Zhao, L. L.; Schatz, G. C. *J. Phys. Chem. B* **2003**, *107*, 668.
(13) Royer, P.; Goudonnet, J. P.; Warmack, R. J.; Ferrell, T. L. *Phys. Rev. B* **1987**, *35*, 3753.
(14) Malinsky, M. D.; Kelly, K. L.; Schatz, G. C.; Van Duyne, R. P. *J. Phys. Chem. B* **2001**, *105*, 2343.
(15) Xu, G.; Tazawa, M.; Jin, P.; Nakao, S.; Yoshimura, K. *Appl. Phys. Lett.* **2003**, *82*, 3811.
(16) Persson, B. N. J. *Surf. Sci.* **1993**, *281*, 153.
(17) (a) Henglein, A. *J. Phys. Chem.* **1993**, *97*, 8457. (b) Henglein, A. *Chem. Rev.* **1989**, *89*, 1861. (c) Linnert, T.; Mulvaney, P.; Henglein, A. *J. Phys. Chem.* **1993**, *97*, 679.
(18) (a) Oldenburg, S. J.; Jackson, J. B.; Westcott, S. L.; Halas, N. J. *Appl. Phys. Lett.* **1999**, *75*, 2897. (b) Oldenburg, S. J.; Jackson, J. B.; Westcott, S. L.; Halas, N. J. *Chem. Phys. Lett.* **1998**, *288*, 243.
(19) Liz-Marzán, L. M.; Giersig, M.; Mulvaney, P. *Langmuir* **1996**, *12*, 4329.
(20) (a) Henglein, A. *Ber. Bunsen-Ges. Phys. Chem.* **1980**, *84*, 253. (b) Henglein, A.; Giersig, M. *J. Phys. Chem.* **1994**, *98*, 6931. (c) Hodak, J. H.; Henglein, A.; Hartland, G. V. *J. Chem. Phys.* **2001**, *114*, 2760.
(21) Sinzig, J.; Radtke, U.; Quinten, M.; Kreibig, U. *Z. Phys. D* **1993**, *26*, 242.
(22) Mulvaney, P.; Giersig, M.; Henglein, A. *J. Phys. Chem.* **1993**, *97*, 7061.
(23) Link, S.; Wang, Z. L.; El-Sayed, M. A. *J. Phys. Chem. B* **1999**, *103*, 3529.
(24) Baba, K.; Ohkuma, Y.; Yonezawa, T.; Miyagi, M. *Appl. Opt.* **2001**, *40*, 2796.
(25) (a) Foss, C. A.; Hornyak, G. L.; Stockert, J. A.; Martin, C. R. *J. Phys. Chem.* **1994**, *98*, 2963. (b) Hornyak, G. L.; Patrissi, C. J.; Martin, C. R. *J. Phys. Chem. B* **1997**, *101*, 1548.
(26) Yu, Y.; Chang, S.; Lee, C.; Wang, C. R. C. *J. Phys. Chem. B* **1997**, *101*, 6661.
(27) (a) Mohamed, M. B.; Link, S.; El-Sayed, M. A. *J. Phys. Chem. B* **1998**, *102*, 9370. (b) Link, S.; Mohamed, M. B.; El-Sayed, M. A. *J. Phys. Chem. B* **1999**, *103*, 3073.
(28) (a) Hulteen, J. C.; Treichel, D. A.; Smith, M. T.; Duval, M. L.; Jensen, T. R.; Van Duyne, R. P. *J. Phys. Chem. B* **1999**, *103*, 3854. (b) Jensen, T. R.; Malinsky, M. D.; Haynes, C. L.; Van Duyne, R. P. *J. Phys. Chem. B* **2000**, *104*, 10549. (c) Haynes, C. L.; Van Duyne, R. P. *J. Phys. Chem. B* **2001**, *105*, 5599.
(29) Petroski, J. M.; Wang, Z. L.; Green, T. C.; El-Sayed, M. A. *J. Phys. Chem. B* **1998**, *102*, 3316.
(30) (a) Jin, R.; Cao, Y.; Mirkin, C. A.; Kelly, K. L.; Schatz, G. C.; Zhang, J. G. *Science* **2001**, *294*, 1901. (b) Jin, R.; Cao, Y.; Hao, E.; Métraux, G. S.; Schatz, G. C.; Mirkin, C. A. *Nature* **2003**, *425*, 487.
(31) (a) Yang, W. H.; Schatz, G. C.; Van Duyne, R. P. *J. Chem. Phys.* **1995**, *103*, 869. (b) Zeman, E. J.; Schatz, G. C. *J. Phys. Chem.* **1987**, *91*, 634. (c) Coronado, E. A.; Schatz, G. C. *J. Chem. Phys.* **2003**, *119*, 3926.
(32) Goodenough, J. B. *J. Solid State Chem.* **1971**, *3*, 490.
(33) (a) Jin, P.; Tazawa, M.; Yoshimura, K.; Igarashi, K.; Tanemura, S.; Macák, K.; Helmersson, U. *Thin Solid Films* **2000**, *375*, 128. (b) Jin, P.; Nakao, S.; Tanemura, S.; Bell, T.; Wielunski, L. S.; Swain, M. V. *Thin Solid Films* **1999**, *343*−*344*, 134.
(34) Marton, J. P.; Lemon, J. R. *Phys. Rev. B* **1971**, *4*, 271.
(35) (a) Granqvist, C. G.; Hunderi, O. *Phys. Rev. B* **1977**, *16*, 3513. (b) Norrman, S.; Andersson, T.; Granqvist, C. G. *Phys. Rev. B* **1978**, *18*, 674. (c) Lee, M. H.; Dobson, P. J.; Cantor, B. *Thin Solid Films* **1992**, *219*, 199.
(36) (a) Link, S.; El-Sayed, M. A. *J. Phys. Chem. B* **1999**, *103*, 4212. (b) Link, S.; El-Sayed, M. A. *J. Phys. Chem. B* **1999**, *103*, 8410.
(37) Palik, E. D. *Handbook of Optical constants of Solids*; Academic Press: San Diego, CA, 1998.
(38) (a) Stockle, R. M.; Deckert, V.; Fokas, C.; Zenobi, R. *Appl. Spectrosc.* **2000**, *54*, 1577. (b) Kim, H. C.; Alford, T. L.; Allee, D. R. *Appl. Phys. Lett.* **2002**, *81*, 4287.